# Minimizing voltage stress in Auxiliary Resonant Commutated Pole Inverters Using saturable Inductors


Markus Zocher
ELSYS, Technische Hochschule Nürnberg
Nuremberg, Germany
Tel. +49 (911) 5880 - 1814
E-Mail: markus.zocher@th-nuernberg.de
URL: http://www.th-nuernberg.de/elsys

Norbert Grass
ELSYS, Technische Hochschule Nürnberg
Nuremberg, Germany
Tel. +49 (911) 5880 - 1814
E-Mail: norbert.grass@th-nuernberg.de
URL: http://www.th-nuernberg.de/elsys

Ralph Kennel
EAL, Technical University of Munich
Munich, Germany
Tel. +49 (89) 289 - 28358
E-Mail: ralph.kennel@tum.de
URL: http://www.epe.ed.tum.de



## Keywords

Resonant converter, Resonant Peak Damping Strategy, Reverse Recovery, Voltage Source Inverter, Zero Voltage Switching



## Abstract

This paper demonstrates a method to reduce the voltage stress of the auxiliary transistors inside an ARCP inverter. A saturable inductance softens the diode reverse recovery process. The proposed method has been successfully tested on a prototype converter over a wide range of currents, DC link voltages and switching frequencies.


## Introduction

Switching losses of semiconductors used in either grid-connected or drive-side inverters are the main limitation to the switching frequency. To allow higher switching frequencies several resonant topologies are known, that can reduce the switching stress of the power semiconductors and allow soft-switching. In contrast to intrinsic resonant topologies like a LLC converter, the Auxiliary Resonant Commutated Pole (ARCP) structure, which has been investigated since the 1990s [1]-[5], adds an auxiliary circuit to a standard two-level-inverter. This circuit provides a resonant phase, which occurs while the main power devices are switched. The standard ARCP structure adds an auxiliary leg to each half-bridge as shown in Fig. 1. In recent years also different ARCP topologies have been published [6][7]. Recently, the company Pre-Switch Inc. presented an ARCP converter based on silicon carbide (SiC) MOSFETs which is controlled by artificial intelligence [9]. Most of the investigations assume a linear or almost linear resonant tank. However, this assumption usually leads to large resonant elements $L_r$ and $C_r$, having a low resonant frequency and therefore limiting the viable switching frequency. This paper shows the challenges of small resonant tanks and the benefits of using a nonlinear partly saturable resonant inductance $L_r$.

## Principle of operation

### Behavior of the ideal circuit

A current commutation from diode $D_2$ to the IGBT $S_1$ with ideal semiconductors is displayed in Fig. 2. When the auxiliary transistor $S_{A1}$ is switched on, the resonant inductance $L_R$ takes over the load current $I_{Ph}$. As soon as $i_R > I_{Ph}$, the bridge output voltage rises and the collector-emitter-voltage of $S_1$ decreases. When the collector-emitter-voltage of the main IGBT $S_1$ reaches zero, $S_1$ is switched on at $t_3$ without significant turn on-losses.

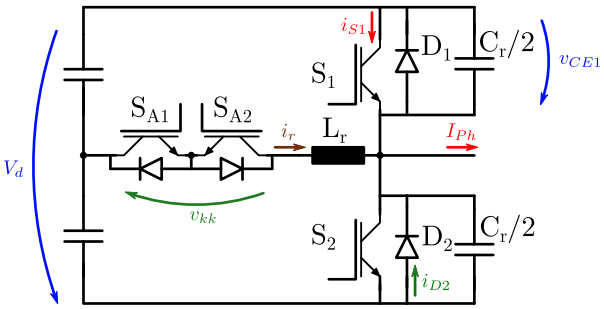


Fig. 1. Schematic half bridge with ARCP

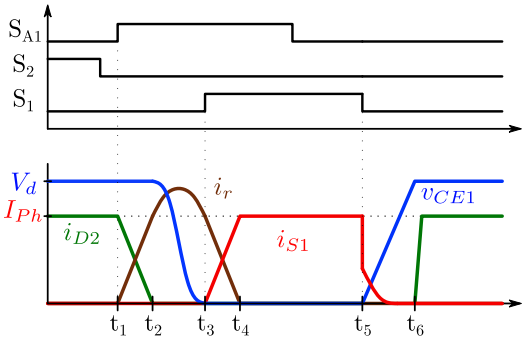


Fig. 2. ARCP idealized waveforms

When the IGBT $S_1$ is turned off, the load current charges the resonant capacitance $C_r$, the rise-time of the collector-emitter-voltage is approximately

$$t_r = t_6 - t_5 = C_r \cdot V_D / I_{Ph} \qquad (1)$$

Since the rise-time of the voltage is increased due to the resonant capacitance, the IGBT's turnoff-losses are lower when compared with a hard switching topology.

However, when the IGBT is turned off at low currents, the rise time $(t_6 - t_5)$ increases substantially like Fig. 3 shows. To fulfil dead-time limitations and avoid a hard turn-on of the main IGBT $S_2$ it might be necessary to speed up the voltage rise. This is done using the auxiliary IGBT $S_{A2}$ (Fig. 4).

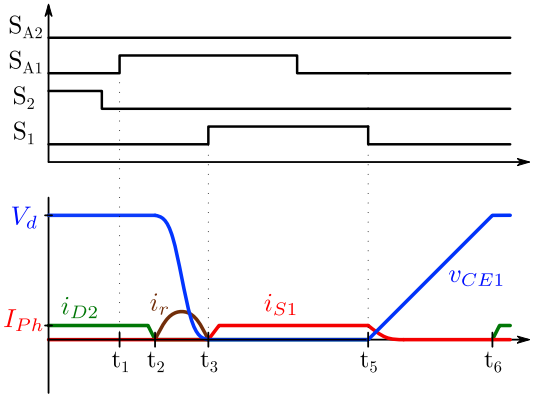


Fig. 3. Waveforms at low current without $S_{A2}$

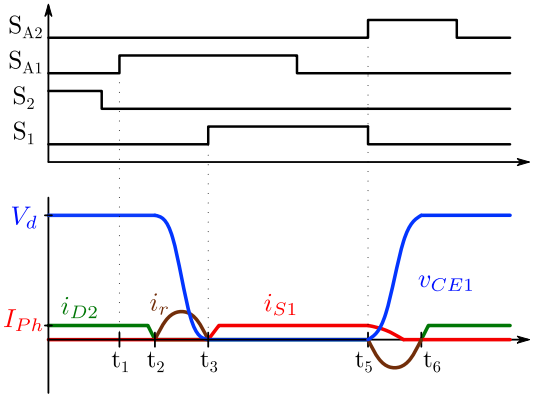


Fig. 4. Waveforms at low current with $S_{A2}$

The turn-off time can be decreased even further at the cost of an increase in switching losses when IGBT $S_{A2}$ is turned on before IGBT $S_1$ is switched off. This operation introducing a "boost" current is discussed in [1].

## Reverse Recovery of auxiliary diodes

The reduction of the ratings of the resonant elements $L_r$ and $C_r$ of an ARCP lead to a faster commutation time, with a lower amount of stored energy, resulting in lower losses in the resonant tank. However, when the inductor $L_r$ is designed with a small inductance value, the reverse recovery behavior of the auxiliary diodes must be considered. During the reverse recovery (starting from $t_4$) the transistors $S_1$ and $S_{A1}$ are constantly switched on and the auxiliary diode of $S_{A2}$ behaves like a nonlinear capacitance. To investigate the reverse recovery behavior, the full circuit can be simplified according to Fig. 5. The capacitance $C_{A2}$ is the sum of the diffusion capacitance containing the charge $Q_a$ and the junction capacitance, which is charged up with $Q_b$.

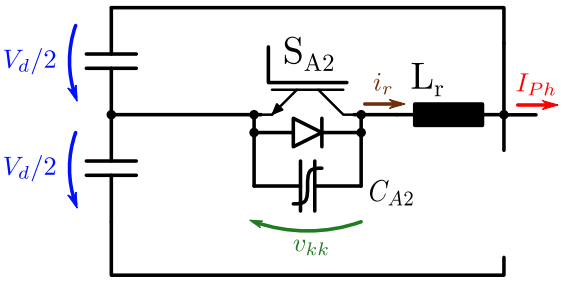


Fig. 5. Schematic during reverse recovery

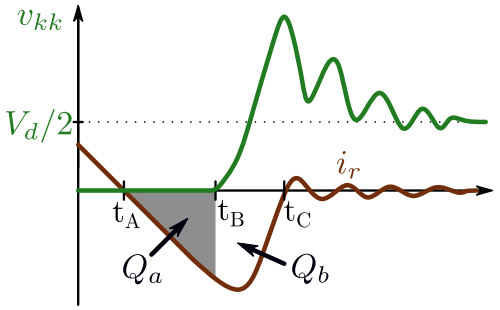


Fig. 6. Waveforms during reverse recovery

Because of the reverse recovery effect, the resonant current $i_r$ can become negative and magnetic energy is stored again in the resonant inductor $L_r$. In Fig. 6 the point $t_4$ of the ideal circuit is expanded to the time range $t_A \dots t_C$.

After removing the charge $Q_a$ the diode is building up the blocking voltage. The magnetic energy is transferred to the resulting output capacitance $C_{A2}$ of the auxiliary IGBT and diode.

The value of the resonant current at $t_B$ can be calculated using the approach

$$\int_{t_A}^{t_B} i_r(t)dt = -\int_{t_A}^{t_B} \frac{V_D}{2 \cdot L_r} dt \stackrel{!}{=} -Q_a \qquad (2)$$

Solved to the current value

$$i_r(t_B) \approx -\sqrt{\frac{V_D \cdot Q_a}{L_r}} \qquad (3)$$

To minimize the stored energy in $L_r$ during reverse recovery, $|i_r(t_B)|$ should be minimized. This can be achieved by choosing a fast recovery diode with small recovery charge or using a large inductance $L_r$.

The voltage and current of the resonant circuit shape between $t_B$ and $t_C$ cannot be calculated straight forward, but the nonlinear capacitance $C_{A2}$ requires the solution of a system of nonlinear differential equations.

## Reduction of diode overvoltage

To keep the conduction losses of the auxiliary elements low and to find fast devices with low $Q_a$, it is desirable to use auxiliary transistors and diodes $S_{A1}$ and $S_{A2}$ with a low blocking voltage. In the best case, the maximum voltage occurring at the auxiliary semiconductor might be lower than the DC link voltage. Therefore, it is important to minimize the overvoltage of $v_{KK}$.

To decrease the overvoltage, the reverse current must be minimized and auxiliary transistors and diodes with a low output capacitance and a low reverse recovery charge should be preferred. However, experimental measurements with an ARCP inverter in the section “Experimental Results” will show that even modern discrete IGBT5 in parallel with fast recovery diodes cause a high overvoltage.

A further solution to lower the overvoltage of $v_{kk}$ would benefit from increased damping of the parasitic resonant tank consisting of $L_r$ and $C_{A2}$, using RC-snubbers and TVS-diodes in parallel to the auxiliary diode. However, adding these elements will add extra losses to the circuit. Moreover, the negative resonant current and consequently the energy stored in $L_r$ will increase, leading to even higher voltage spikes. As adding RC-snubbers and TVS-diodes will create new disadvantages, this approach is not discussed further.

The presented approach starts from the fact, that the reverse recovery current will decrease, when the negative slope of the resonant current $i_r$ is decreased. At a given DC link voltage this can be achieved using a larger resonant inductance $L_r$. Since this large inductance value is only needed for resonant currents close to zero, a combination of a linear and a saturable inductance is promising to decrease the

reverse current and maintain the benefits of a small inductance. With this combination, the benefits of using a small resonant tank are maintained and the reverse recovery process is optimized.

The saturable part of the inductance can be built using a core with high permeability e.g., the standard ferrite N87 from TDK [12], the linear part using low permeability materials like iron powder.

As the flux density inside the ferrite core is expected to change fast, the eddy current losses inside the ferrite core provide extra damping while the ferrite core is not saturated. Therefore, the saturable inductor additionally works as a magnetic snubber in the critical moment. A similar technique is already known for resonant DC-DC-converters [11].

### Temperature dependency of saturable core

For practical experiments ferrite cores with the material N87 from the manfacturer EPCOS TDK were used. Fig. 7 which was extracted from [12] shows, that the core saturates more quickly at higher temperatures. Moreover, the loss density decreases at high temperatures according to Fig. 8 . A small loss density is equivalent to a lower imaginary part of the complex permeability and thus, providing less damping. Therefore, the ferrite core should be chosen regarding satisfactory behavior at high temperatures.

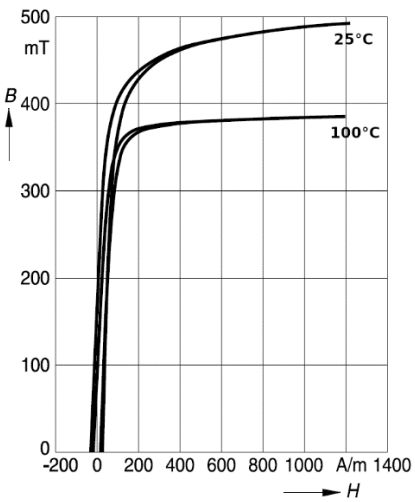


Fig. 7. N87 Saturation [12]

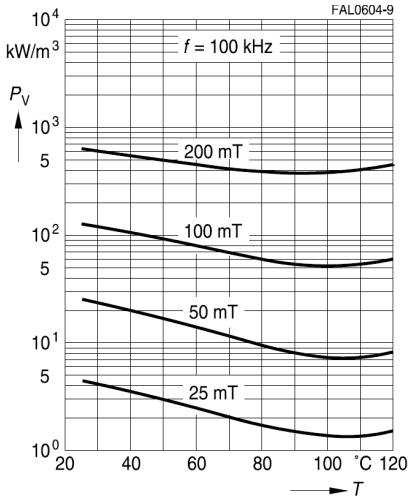


Fig. 8. N87 Loss density [12]

## Experimental Results

For practical verification, a three-phase two-level inverter with ARCP extension has been built.

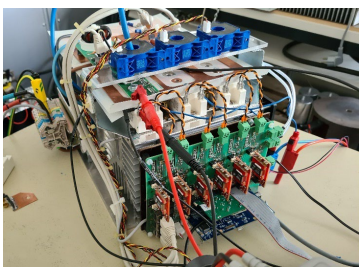

Fig. 9. Converter Prototype

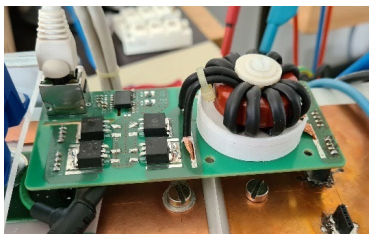

Fig. 10. Auxiliary Leg without saturable core

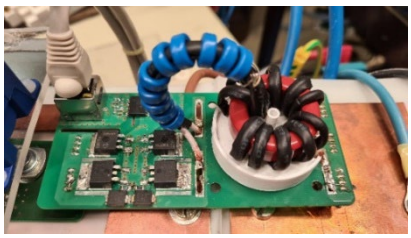

Fig. 11. Auxiliary Leg with saturable core

Fig. 10 and Fig. 11 show the auxiliary legs that are compared. The linear core is identical, the saturable inductor contains 10 extra N87 ferrite cores. Small cores are used as the ratio between surface area and core volume is high. Therefore, the dissipation of the heat resulting from the core losses is more effective. Simulating the behavior of the complete circuit is difficult, since a detailed nonlinear model of the N87 ferrite core and a detailed diode model containing the reverse recovery behavior is needed. Therefore, a more practical approach was preferred for selecting the ferrite cores.
The number of ferrite cores was selected in a way that the resulting inductance without saturation is at least 10 times as high as in the saturated case. The following table gives an overview of the used components.

**TABLE I. Components Prototype Converter**

| Component | Type | Max. Voltage | Nom. Current |
|---|---|---|---|
| Main IGBTs | Semikron SKM100GB12T4 | 1200V | 100A |
| Auxiliary IGBTs | Infineon IGB50N65S5 | 650V | 50A |
| Auxiliary Diodes | Vishay ETH3006S | 600V | 30A |
| DC link | Kemet C44UM: 1100uF | 1200V | 114A |
| Resonant Inductance (linear) | Carbonyl Iron Powder Core, Amidon (T130-2): ≈ 650 nH | | |
| Resonant Inductance (nonlinear) | 10x Epcos N87 Core (T10): ≈ 9.0 uH | | |
| Resonant Capacitance $(C_r/2)$ | Two 1206 2.2nF (NP0) in series | 2x630V | |

Since the timing of the auxiliary leg cannot be calculated straight forward the method proposed in [10] is used. For double pulse measurements an inductive load was connected between DC+ and the bridge output of one half bridge, the measurements with periodic signals were done in a full-bridge configuration.

## Double Pulse Measurements

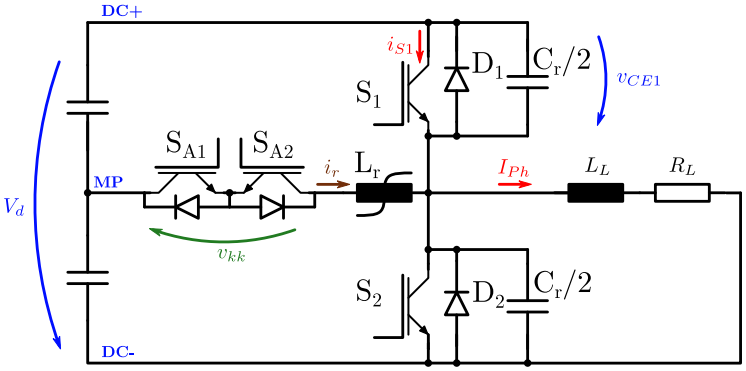


Fig. 12. Double pulse setup

The behavior of the linear and the saturable inductors are compared using double-pulse measurements. Fig. 13 shows the collector-emitter-voltages and the collector currents of the main transistor $S_1$ which only subtly differ.
As it can be seen from Fig. 14, the linear inductor causes a large overvoltage at the resonant transistors. At a DC link voltage of 500V the maximum overvoltage of $v_{kk}$ reaches 574V (green waveform of Fig. 14) which is close to 600V - the maximum blocking voltage of the auxiliary diode. With the extra saturable inductor, the maximum voltages could be reduced down to 273V (blue waveform of Fig. 14) which is only slightly higher than half of the DC link voltage. Since the ferrite cores saturate quickly, the overall commutation time is not increased significantly.

As inverters with 1200V IGBTs are usually used up to a DC link voltage of about 800V, the operation of an ARCPI with a linear inductance that provides a small commutation time and auxiliary transistors of the 600V/650V class is not feasible. However, with the saturable core the DC link voltage of 800V is achievable.

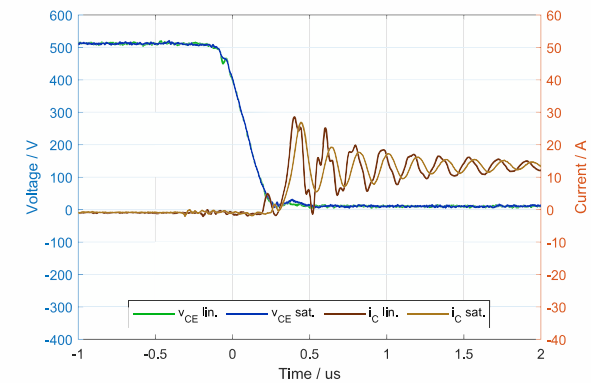


Fig. 13. Double Pulse Measurements, $V_D = 500\,V$, $I_{Ph} = 15\,A$, main circuit

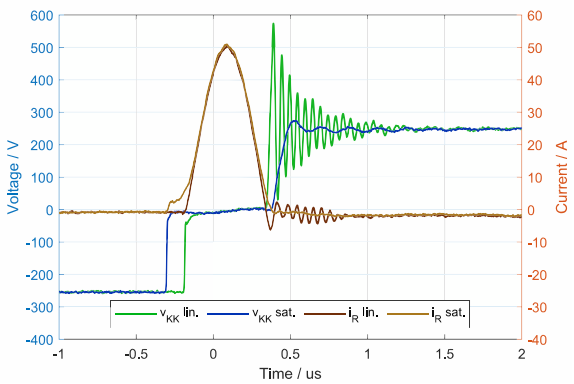


Fig. 14. Double Pulse Measurement, $V_D = 500\,V$, $I_{Ph} = 15\,A$ resonant circuit

## Loss Estimation

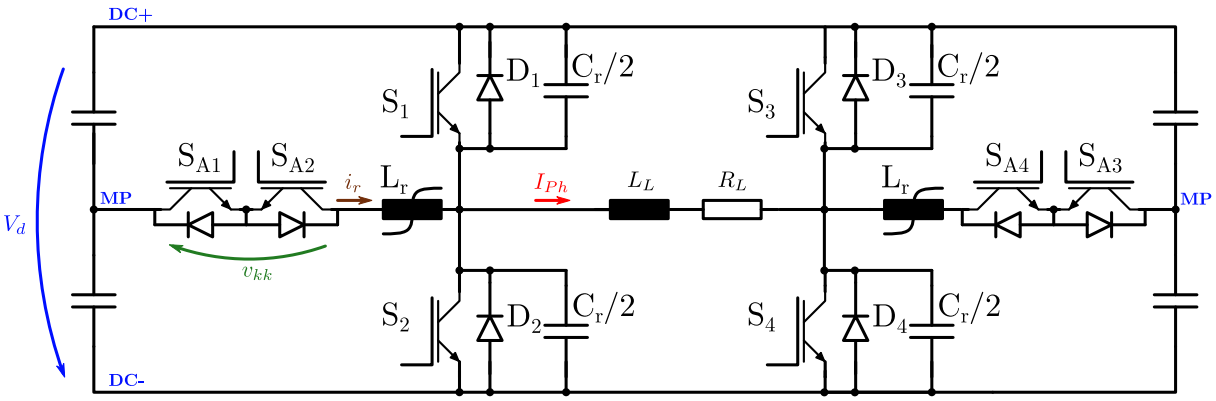


Fig. 15. Periodic operation setup

The improvement in the system behavior comes at the expense of losses inside the ferrite core. To estimate the losses, the ARCP converter is switched periodically in full bridge configuration with an inductive load ($L_L \approx 1mH$) between two phase legs and a 50Hz sinusoidal current with the amplitude $I_L$.

$$I_{Ph}(t) = \mathrm{I_L} \cdot \sin\left(2\pi \cdot 50\mathrm{Hz} \cdot \mathrm{t}\right) \qquad (4)$$

A direct loss measurement in the electrical domain using voltage and current measurements was found to be too inaccurate, therefore a calorimetric measurement is preferred. During operation the temperature is measured with an infrared camera. The following thermal properties were obtained for a single toroid core (R10x6x4) using the cool down behavior from [13]. The temperature was measured with an infrared camera and an additional K-type thermocouple. A single ferrite core has the following thermal properties

$$C_{th} \approx 0.72\frac{\mathrm{J}}{\mathrm{K}}, \tau_{th} \approx 80s \rightarrow\ R_{th} = \frac{\tau_{\mathrm{th}}}{\mathrm{C_{th}}} \approx 110\frac{\mathrm{K}}{\mathrm{W}} \qquad (5)$$

At an ambient temperature of 22°C a temperature of 100°C of the hottest core equals a loss of 700mW. In this case, the sum of the losses of all 10 ferrite cores is less or equal to 7.0W per phase. However, it was already shown [10] with the same prototype that the turn on losses are reduced from 15mJ to less than 500µJ at the nominal operating point ($V_d = 600V$ and $I_C = 100A$).

Therefore, the extra losses generated from the saturable core are neglectable compared to the savings in switching losses in a hard-switched inverter.

## Parameter Sweeps

Fig. 16 illustrates that the temperature of the ferrite core increases linearly with the switching frequency. This behavior is like expected since the core losses are proportional to the number of saturation cycles.

A higher DC link voltage leads to a faster saturation and higher eddy currents inside the ferrite. The measurements in Fig. 17 show, that the core temperature increases almost linearly with the DC link voltage.

The load current dependency on the temperature displayed in Fig. 18 might seem unintuitive at first glance. At higher output current amplitudes, the ferrite core stays cooler. This is caused by the switching actions when the current is commutated from an IGBT to the complimentary diode. At low currents the turn off must be accelerated using the auxiliary circuit like displayed in Fig. 4. When the amplitude of the sinusoidal output current is high, this speed-up is only needed during the zero crossings of the output current and not at each switching action.

In summary, the highest losses in the saturable core occur at the highest DC link voltage, the highest switching frequency and low output current amplitudes, which is the most critical point of operation.

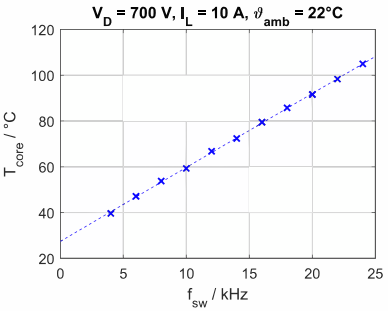


Fig. 16. $f_{sw}$ dependency on $T_{Core}$

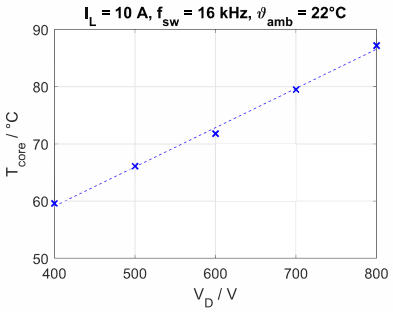


Fig. 17. $V_d$ dependency on $T_{Core}$

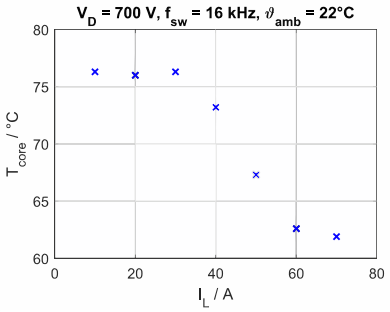


Fig. 18. $I_L$ dependency on $T_{Core}$

## Temperature dependency of ferrite

Like explained in the theoretical part of this paper, it is important to consider the temperature dependency of the ferrite core itself. The saturation flux density as well as the core losses of N87 material decrease when the temperature increases from 25°C to 100°C [12]. These two effects lead to a larger overvoltage at higher core temperature. A periodic operation at 700V, 22kHz and a low output current amplitude of 15A leads to a core temperature of approximately 100°C like the thermal measurement in Fig. 19 shows. The according current and voltage signals at this point is shown in Fig. 20 and compared to a measurement at 25°C. The maximum voltage increases from 402V to 510V. Compared to the maximum blocking voltage of 600V, this voltage spike is still acceptable.

Therefore, it must be ensured, that the auxiliary voltage is below the maximum blocking voltage at the largest ambient temperature in combination with the most critical point of operation.

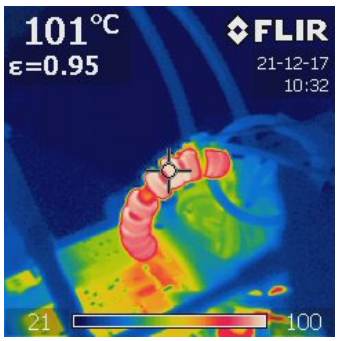


Fig. 19. Thermal camera, $V_D = 700\,V$, $f_{sw} = 22kHz$, $I_{Ph} = 15\,A$

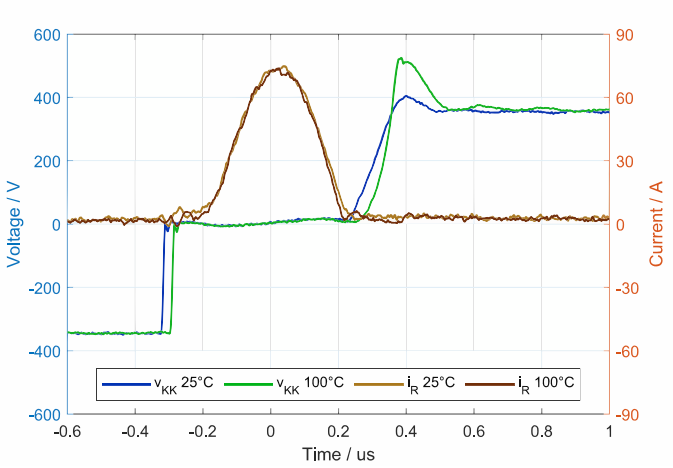


Fig. 20. $V_D = 700\,V$, $I_{Ph} = 15\,A$, comparison temperature behaviour of nonlinear resonant circuit

## Conclusion

This paper showed that a saturable core, working as a magnetic snubber, significantly reduces the overvoltage, which results from the reverse recovery of the auxiliary diodes, inside the auxiliary leg of a ARCP inverter. This allows ARCP designs with smaller resonant tanks and higher switching frequencies, where the reverse recovery behavior of the ARCP diodes is critical. The resulting core losses are usually small, compared to the rated power and the savings in switching losses of the inverter, but the temperature must be considered for the saturation and damping behavior of the saturable core. The most critical operation point is at the highest switching frequency and DC link voltage and low output currents. This operation point can be used to investigate and optimize the design of the partial saturable inductor.

## References

[1] R.W. De Doncker and J.P. Lyons: “The Auxiliary Resonant Commutated Pole Converter”.Proceedings IEEE-IAS, Seattle, pp. 1228-1235, 1990

[2] H.-J. Pfisterer and H. Spath, "Switching behaviour of an auxiliary resonant commutated pole (ARCP) converter," *7th IEEE International Power Electronics Congress. Technical Proceedings. CIEP 2000 (Cat. No.00TH8529)*, 2000, pp. 359-364, doi: 10.1109/CIEP.2000.891440.

[3] R. Teichmann and H. Gueldner: "Analysis of transfer ratio limitations in auxiliary resonant commutated pole converters," *7th IEEE International Power Electronics Congress. Technical Proceedings. CIEP 2000 (Cat. No.00TH8529)*, 2000, pp. 15-20, doi: 10.1109/CIEP.2000.891385.

[4] R. Teichmann, "Control parameter selection in auxiliary resonant commutated pole converters," *IECON'01. 27th Annual Conference of the IEEE Industrial Electronics Society (Cat. No.37243)*, 2001, pp. 862-869 vol.2, doi: 10.1109/IECON.2001.975870.

[5] F. Hinrichsen and G. Tareilus: “Simple Design and Control of ARCP-Inverter for Universal Power Range”, SPEEDAM, Ravello, 2002

[6] H. Morii, M. Yamamoto and S. Funabiki, "Capacitor-Less Auxiliary Resonant Commutated Pole (ARCP) voltage source soft switching inverter suitable for EV," *2009 13th European Conference on Power Electronics and Applications*, 2009, pp. 1-8.

[7] E. Chu, L. Huang and Z. Fu, "Research on an active double auxiliary resonant commutated pole soft-switching inverter," 2014 IEEE 23rd International Symposium on Industrial Electronics (ISIE), 2014, pp. 637-642, doi: 10.1109/ISIE.2014.6864686.

[8] A. Charalambous, X. Yuan, N. McNeill, S. Walder, Q. Yan and C. Frederickson, "Controlling the output voltage frequency response of the auxiliary commutated pole inverter," *IECON 2016 -*

*42nd Annual Conference of the IEEE Industrial Electronics Society*, 2016, pp. 3305-3310, doi: 10.1109/IECON.2016.7793828.

[9] Pre-Switch Inc.: “Pre-Switch demonstrates efficacy of AI-based soft switching using 200kVA inverter reference”, https://www.pre-switch.com, 2021

[10] M. Zocher, N. Grass and R. Kennel, "Auxiliary Resonant Commutated Pole Inverter (ARCPI) Operation Using online voltage measurements," 2022 IEEE Applied Power Electronics Conference and Exposition (APEC), 2022, pp. 1592-1597, doi: 10.1109/APEC43599.2022.9773560.

[11] K. Harada, Y. Ishihara and Toshiyukitodaka, "An improved magnetic snubber circuit for the diode reverse recovery in DC-to-DC converters," PESC 98 Record. 29th Annual IEEE Power Electronics Specialists Conference (Cat. No.98CH36196), 1998, pp. 701-706 vol.1, doi: 10.1109/PESC.1998.701975.

[12] TDK Epcos, Datasheet N87 Ferrite, https://www.tdk-electronics.tdk.com/en/529404/products/product-catalog/ferrites-and-accessories/epcos-ferrites-and-accessories/ferrite-materials

[13] P. Papamanolis, T. Guillod, F. Krismer and J. W. Kolar, "Transient Calorimetric Measurement of Ferrite Core Losses up to 50 MHz," in IEEE Transactions on Power Electronics, vol. 36, no. 3, pp. 2548-2563, March 2021, doi: 10.1109/TPEL.2020.3017043.